Superstructural Model for Small-Angle X-ray Scattering: Application to Nylon 6 Fiber

Zeyong Zheng, Shuichi Nojima, Takashi Yamane, and Tamaichi Ashida*

Department of Applied Chemistry, Faculty of Engineering, Nagoya University, Nagoya 464-01, Japan. *Received November 19, 1988; Revised Manuscript Received March 30, 1989*

ABSTRACT: A model for the superstructure of fibers has been presented to explain the small-angle X-ray scattering (SAXS) intensity, in which the three-dimensional paracrystalline theory by Hosemann is combined with the inclined lamella structure model proposed by Keller and a distribution function is introduced to describe the cluster orientation about its own axis. By use of this model the SAXS pattern of nylon 6 fiber has been analyzed, and reasonable results were obtained for the parameters characterizing the superstructure of the fiber, such as macrolattice dimensions, fluctuations, and orientation distributions.

Introduction

Although qualitative or semiquantitative studies have been extensively carried out, there have been limited investigations devoted to the quantitative aspect of the morphologies of the oriented samples found by the small-angle X-ray scattering (SAXS) technique. The limited works done so far include those on linear polyethylene,[1,2] isotactic polypropylene,[3,4] low-density polyethylene,[5,6] and isotactic polybutene.[7] Most of these investigations are based on the paracrystalline theory of Hosemann et al.[8,9] They proposed a paracrystal model[10,11] based on three-dimensional coherence between crystallites to interpret the SAXS pattern from oriented samples. According to the theory, the crystallites interfere with each other not only longitudinally but also laterally, constituting a paracrystalline macrolattice (superlattice) in real space. The frequently occurring lamellar and fibrillar structures are the special cases of such a superlattice. It acts as a lamellar structure when the lateral distance between crystallites is small enough to be neglected (refer to Figure 5, left, in ref 13) and acts as a fibrillar structure if the crystallites are well aligned longitudinally (refer to Figure 5, right, in ref 13). For a lamellar structure, the lamellar stack is composed of a number of fibrils that cohere laterally with each other. The inclination of the mean lamellar surface depends on the width of the fibril and relative longitudinal displacement of neighbors. Since the 001 reflections of the superlattice account for the SAXS pattern, a two-point diagram is realized by an orthorhombic lattice ($\beta = 90°$, see Figure 5 in ref 13) and a four-point diagram by a monoclinic one ($\beta \neq 90°$).

On the basis of the paracrystalline model, Wilke et al.[6,12,13] proposed a superstructural model for uniaxially oriented polymers, in which the orientation distribution of the crystallites is taken into account. According to the model, the real sample consists of a large number of clusters of crystallites, orientation of the cluster axis with respect to the fiber axis is distributed following a certain density function, and the cluster orientation about its own axis follows uniform distribution (cylindrically symmetrical distribution). This model was used successfully in analyzing the SAXS patterns from uniaxially oriented low-density polyethylene.[6]

To explain the four-point SAXS diagram, Keller et al.[14-17] proposed a qualitative model in which the lamellae are stacked along the fiber axis with the normals to their surfaces inclined at an angle that is equal to one-half of the splitting angle between the diffraction lobes. This model was employed by many other investigators[18-20] to conduct quantitative calculation. But in all of these investigations, the probable coherence between neighboring lamellar stacks was not taken into account.

In a previous paper,[21] the superstructural model presented by Wilke et al.[6,12,13] based on the paracrystalline theory was employed to analyze the two-point SAXS pattern of oriented nylon 6 at swelling equilibrium, and several significant results have been obtained. This model failed, however, to explain the four-point SAXS diagram of the nylon 6 fiber. We would attribute this inability to the conflict that may occur between Hosemann and Keller models in the case of a four-point diagram (i.e., the lamellar structure of the Hosemann model will not be true if the lateral distance between the fibrils is not small) and the limitation of the uniform distribution assumption on the cluster orientation about its own axis.

In the present work, a new model is proposed in which the inclined lamella structure model by Keller et al. is incorporated as well as the paracrystalline theory of Hosemann and then a distribution function is introduced to describe the cluster orientation about its own axis. The combination of the two models may be expected to make clear some uncertainties[22] such as the coherence in the direction transverse to the axes of lamellae stacks. Our model is then applied to the nylon 6 fiber, which produces a SAXS pattern with four-point character,[23] to examine its validity.

Theory

Basic Scattering Unit. According to the paracrystalline theory, the crystallites cohere not only in the longitudinal direction but also in the lateral one, thus constituting a paracrystalline macrolattice, which is called a basic scattering unit. Then, on the basis of Keller's model,[14-17] the crystallite can be considered to be a lamella with inclined surface in the case of the four-point SAXS diagram. Therefore, if incorporating the consideration of Keller et al., the basic scattering unit can be thought of as a three-dimensional paracrystalline monoclinic macrolattice composed of identical lamellae with inclined surfaces as illustrated in Figure 1, where $\mathbf{n}$ is parallel to $\mathbf{a}_3$ and is called the cluster axis. The real sample can be pictured as consisting of a large number of such basic scattering units with various orientations.

Coordinate Systems. The following three coordinate systems, as shown in Figure 2, are required in order to deal with various components of orientation of the crystallites and to calculate various averages over whole space. The first is necessary for fixing the space, the second for specifying the orientation of $\mathbf{a}_1$ of the basic scattering unit about $\mathbf{n}$, and the third for the convenience to represent the scattered intensity by such a single unit.

(i) (r, θ, φ): This is the space-fixing coordinate system, with the fiber axis $\mathbf{f}$ as the polar axis. For the sake of convenience, the cluster axis $\mathbf{n}$ is located at $\varphi = 0$. So the

0024-9297/89/2222-4362$01.50/0

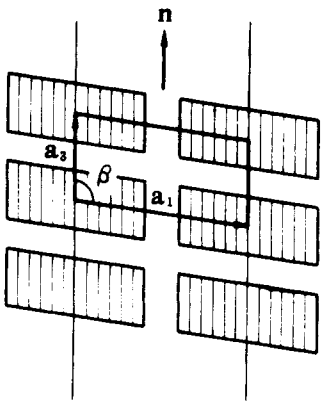

Figure 1. Illustration of the paracrystalline macrolattice composed of lamellae with inclined surfaces: $\mathbf{a}_1$ parallel to lamellar surface, $\mathbf{a}_3$ lateral to surface or molecular chains, and $\mathbf{a}_2$ perpendicular to paper plane; $\mathbf{n}$ is parallel to $\mathbf{a}_3$ and is called the cluster axis.

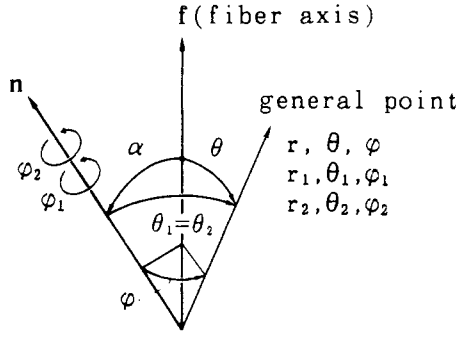

Figure 2. Definition of coordinate systems in real space.

direction of $\mathbf{n}$ is determined by $\varphi = 0$ and α, the angle between $\mathbf{n}$ and $\mathbf{f}$ (Figure 2).

(ii) $(r_1, \theta_1, \varphi_1)$: The polar axis is given by $\mathbf{n}$, and the plane defined by $\mathbf{n}$ and $\mathbf{f}$ specifies $\varphi_1 = 0$ (Figure 3).

(iii) $(r_2, \theta_2, \varphi_2)$: This is the coordinate system defined within the basic scattering unit, also with $\mathbf{n}$ as polar axis, but $\varphi_2 = 0$ is now determined by the plane defined by $\mathbf{n}$ and $\mathbf{a}_1$ (also see Figure 3).

The same origin is chosen for all three coordinate systems, so that $r = r_1 = r_2$. The coordinate systems in reciprocal space such as $(r^*, \theta^*, \varphi^*)$ are defined with the same orientation as in real space.

As shown in Figure 3, the orientation of a basic scattering unit in space is specified by α and δ, the latter being the angle between the plane defined by $\mathbf{n}$ and $\mathbf{f}$ ($\varphi_1 = 0$) and that by $\mathbf{n}$ and $\mathbf{a}_1$ ($\varphi_2 = 0$), and thus determines the orientation of $\mathbf{a}_1$ about $\mathbf{n}$ in the $(r_1, \theta_1, \varphi_1)$ system. The intensity distribution of such a single scattering unit is to be expressed as $i_1(r^*_2, \theta^*_2, \varphi^*_2)$.

General Intensity Formula. To calculate the SAXS intensity we introduce several assumptions about the distribution of the orientation of the basic scattering unit. (A) The cluster orientation of $\mathbf{a}_1$ about $\mathbf{n}$ is described by a function $Q(\delta)$ with its maximum at $\delta = 0$ (Figure 3). (B) The distribution of the orientation of $\mathbf{n}$ with respect to $\mathbf{f}$ is given by a function $D(\alpha)$. (C) The distribution of $\mathbf{n}$ about $\mathbf{f}$ shows rotational symmetry, which is equivalent to saying that $D(\alpha)$ is a rotationally symmetrical function.

According to assumption A, the averaged intensity $\bar{I}$ at a general point in the $(r^*_1, \theta^*_1, \varphi^*_1)$ system can be obtained by integrating $i_1(r^*_2, \theta^*_2, \varphi^*_2)$ with respect to δ and taking into account the distribution density $Q(\delta)$:

$$\bar{I}(r^*_1, \theta^*_1, \varphi^*_1) = \int_{-\pi}^{\pi} i_1(r^*_2, \theta^*_2, \varphi^*_2) Q(\delta)\, \mathrm{d}\delta \qquad (1)$$

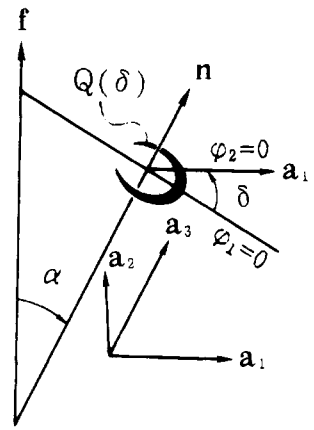

Figure 3. Schematic representation of the distribution $Q(\delta)$ of the orientation of $\mathbf{a}_1$ about $\mathbf{n}$ with its maximum at $\delta = 0$. If the $\mathbf{a}_3$ axis is superimposed on $\mathbf{n}$, δ is then visualized as the angle between the plane defined by $\mathbf{f}$ and $\mathbf{n}$ and that by $\mathbf{n}$ and $\mathbf{a}_1$.

To conduct this integration the coordinates in the $(r^*_2, \theta^*_2, \varphi^*_2)$ system must be reduced to those in the $(r^*_1, \theta^*_1, \varphi^*_1)$ system. From the above definitions on the coordinate systems along with Figure 3, it follows immediately that

$$r^*_2 = r^*_1 \qquad (2a)$$

$$\theta^*_2 = \theta^*_1 \qquad (2b)$$

$$\varphi^*_2 = \varphi^*_1 - \delta \qquad (2c)$$

Likewise, before calculating the intensity $\bar{I}_{av}$ at a general point in the $(r^*, \theta^*, \varphi^*)$ system, we have further to transform the coordinates from the $(r^*_1, \theta^*_1, \varphi^*_1)$ to the $(r^*, \theta^*, \varphi^*)$ system. By means of proper geometrical derivation, we have

$$r^*_1 = r^* \qquad (3a)$$

$$\cos\theta^*_1 = \cos\alpha\cos\theta^* + \sin\alpha\sin\theta^*\cos\varphi^* \qquad (3b)$$

$$\cos\varphi^*_1 = (-\sin\alpha\cos\theta^* + \cos\alpha\sin\theta^*\cos\varphi^*)/\sin\theta^*_1 \qquad (3c)$$

On the basis of assumption B, $\bar{I}_{av}(r^*, \theta^*, \varphi^*)$ can be written as follows, taking into account eq 3a–c:

$$\bar{I}_{av}(r^*, \theta^*, \varphi^*) = \int_0^{\pi} \bar{I}(r^*_1, \theta^*_1, \varphi^*_1) D(\alpha) \sin\alpha\, \mathrm{d}\alpha \qquad (4)$$

Finally, according to assumption C, the experimentally measurable intensity $I(r^*, \theta^*)$ can be obtained by averaging $\bar{I}_{av}(r^*, \theta^*, \varphi^*)$ against φ^* over the range 0–2π, i.e.

$$I(r^*, \theta^*) = \int_0^{2\pi} \bar{I}_{av}(r^*, \theta^*, \varphi^*)\, \mathrm{d}\varphi^* \qquad (5)$$

If eq 1 is inserted into eq 4 and then eq 4 into eq 5, therefore, the final expression of $I(r^*, \theta^*)$ becomes

$$I(r^*, \theta^*) = \int_0^{2\pi}\int_0^{\pi}\int_{-\pi}^{\pi} i_1(r^*_2, \theta^*_2, \varphi^*_2) Q(\delta) D(\alpha) \sin\alpha\, \mathrm{d}\delta\, \mathrm{d}\alpha\, \mathrm{d}\varphi^* = \int_0^{2\pi}\int_0^{\pi}\int_{-\pi}^{\pi} I_1(\mathbf{b}) Q(\delta) D(\alpha) \sin\alpha\, \mathrm{d}\delta\, \mathrm{d}\alpha\, \mathrm{d}\varphi^* \qquad (6)$$

where $I_1(\mathbf{b}) = i_1(r^*_2, \theta^*_2, \varphi^*_2)$ is the scattered intensity by a single basic scattering unit, $\mathbf{b}$ being the scattering vector in the $(r^*_2, \theta^*_2, \varphi^*_2)$ system. The resulting $I(r^*, \theta^*)$ represents relative intensity.

To carry out numerical calculation of eq 6, $I_1(\mathbf{b})$, $Q(\delta)$, and $D(\alpha)$ should be replaced by actual numerical functions. In relation to the distributions of the cluster orientation, it is a common practice to assume the Gaussians, which are centered at $\delta = 0$ for the distribution of $\mathbf{a}_1$ about $\mathbf{n}$ and

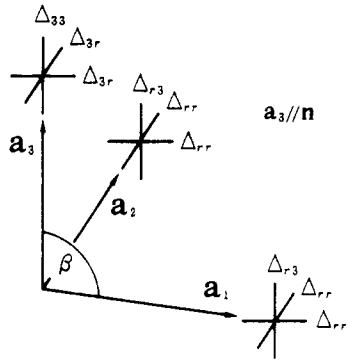

Figure 4. Lattice fluctuation parameters. The subscript **r** denotes the direction transverse to $\mathbf{a}_3$. The same values are usually assumed for $\mathbf{a}_1$ and $\mathbf{a}_2$ if fiber symmetry exists.

at $\alpha = 0$ in the case of highly oriented fiber for that of **n** relative to **f** respectively as

$$Q(\delta) = \frac{1}{(2\pi)^{1/2}\sigma_d} \exp\left[-\frac{1}{2}\left(\frac{\delta}{\sigma_d}\right)^2\right] \tag{7}$$

$$D(\alpha) = \frac{1}{(2\pi)^{1/2}\sigma_\alpha} \exp\left[-\frac{1}{2}\left(\frac{\alpha}{\sigma_\alpha}\right)^2\right] \tag{8}$$

where σ_d and σ_α are the half-height widths of the two distributions, respectively.

With the aid of the above assumption on the structure of the basic scattering unit, $I_1(\mathbf{b})$ can be given by[9,24]

$$I_1(\mathbf{b}) = |F(\mathbf{b})|^2 Z(\mathbf{b}) \tag{9}$$

where $F(\mathbf{b})$ is the scattered amplitude by a single crystallite constituting the macrolattice. For a lamellar crystallite with inclined surface, $|F(\mathbf{b})|^2$ can be expressed by

$$|F(\mathbf{b})|^2 = \exp\{-\pi[L_1^2(b_1 \sin\beta + b_3\cos\beta)^2 + L_2^2 b_2^2 + L_3^2 b_3^2]\} \sin^2\beta \tag{10}$$

where b_1, b_2, and b_3 are reciprocal Cartesian coordinates in the $(r^*_2, \theta^*_2, \varphi^*_2)$ system, L_1, L_2, and L_3 are the lengths of the three edges of the lamella, and β is the angle between lateral and basal (folding) planes of the lamella. Details of the derivation of eq 10 are given in the Appendix.

On the other hand, $Z(\mathbf{b})$ is the lattice factor of an ideal three-dimensional paracrystalline macrolattice[9,24] given by

$$Z(\mathbf{b}) = \prod_{k=1}^{3} \frac{1 - |F_k|^2}{1 + |F_k|^2 - 2|F_k|\cos(2\pi\mathbf{b}\cdot\mathbf{a}_k)} \tag{11}$$

$$|F_k| \equiv |F_k(\mathbf{b})| = \exp[-2\pi^2 \mathbf{b}\cdot\mathbf{T}(k)\cdot\mathbf{b}] \tag{12}$$

where $\mathbf{T}(k)$ is the fluctuation tensor, whose principal elements consist of $\Delta_{ii}(k)$,[25] the fluctuations of the lattice points (Figure 4).

For uniaxially oriented samples with rotational symmetry about the fiber axis, the monoclinic macrolattice[6,25] is usually utilized to calculate the four-point SAXS pattern. For such a case, the terms $\mathbf{b}\cdot\mathbf{T}(k)\cdot\mathbf{b}$ and $\mathbf{b}\cdot\mathbf{a}_k$ can be expanded as follows:[6,25]

$$\mathbf{b}\cdot\mathbf{T}(1)\cdot\mathbf{b} = (b_r a_r g_{rr})^2 + (b_3 a_3 g_{r3})^2 \tag{13a}$$

$$\mathbf{b}\cdot\mathbf{T}(2)\cdot\mathbf{b} = (b_r a_r g_{rr})^2 + (b_3 a_3 g_{r3})^2 \tag{13b}$$

$$\mathbf{b}\cdot\mathbf{T}(3)\cdot\mathbf{b} = (b_r a_r g_{3r})^2 + (b_3 a_3 g_{33})^2 \tag{13c}$$

and

$$\mathbf{b}\cdot\mathbf{a}_1 = (b_1 + b_3\cot\beta)a_r \tag{14a}$$

$$\mathbf{b}\cdot\mathbf{a}_2 = b_2 a_r \tag{14b}$$

$$\mathbf{b}\cdot\mathbf{a}_3 = b_3 a_3 \tag{14c}$$

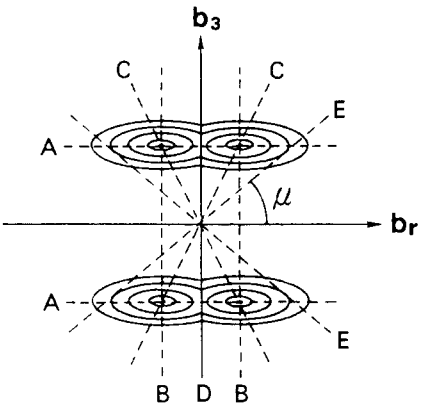

Figure 5. Sections on the SAXS pattern used in the model fitting: section A, parallel to the equator and through the intensity maximum; section B, parallel to the meridian and through the intensity maximum; section C, through the origin and the intensity maximum; section D, along the meridian; section E, through the origin with the azimuth μ equal to 35°.

where $a_r = a_2 = a_1 \sin\beta$, $b_r^2 = b_1^2 + b_2^2$, and g's are the relative fluctuations defined by

$$g_{rr} = \Delta_{rr}/a_r \qquad g_{r3} = \Delta_{r3}/a_3 \qquad g_{3r} = \Delta_{3r}/a_r \qquad g_{33} = \Delta_{33}/a_3 \tag{15}$$

where Δ's are the absolute statistical fluctuations shown in Figure 4; for instance, Δ_{r3} represents the fluctuation of cell vector $\mathbf{a}_1$ (or $\mathbf{a}_2$) in the direction of $\mathbf{a}_3$ and so on.

Experimental Section

Preparation of SAXS Pattern. The SAXS pattern of nylon 6 fibers in their as-spun form was recorded photographically in a X-ray film with a SAXS camera with pinhole collimation and a rotating anode X-ray generator (RIGAKU) operated at 50 kV, 80 mA. The SAXS pattern was digitalized with an optical densitometer, and the intensity profiles along the special sections (A–E) illustrated in Figure 5 were obtained with the averages taken over all four quadrants. The intensity profiles thus obtained were then smoothed with a stepwise cubic least-squares routine to minimize the statistical error. Standard deviations over all four quadrants were taken as a measure of the error of the intensity measurement. The mean error thus estimated was less than 7%.

Two-Dimensional Analysis of SAXS Intensity. The superstructure parameters for the model were obtained by fitting the calculated intensity based on eq 6 to the observed one using the least-squares method with a Gauss–Newton algorithm. The fitting was performed for the five sections specified above. For highly oriented low-density polyethylene, comparison between experimental and theoretical SAXS profiles along three special sections (A, B, C) yields reasonable parameters.[6] We found in the case of the nylon 6 fiber, however, that it is insufficient to carry out fitting only for the three sections because remarkable deviations would be observed for sections D and E even if good agreements were obtained for the remaining sections. In addition, although there are as many as 10 independent superstructure parameters in the model, as listed in Table I, only 6–10 data points along each section will be sufficient to determine these parameters by least-squares fitting. This is justified by the fact that the intensity profile of each section just affects a special set of parameters, as discussed in ref 13; section B, for example, affects dominantly the parameters a_3, H, and g_{33}, and so on.

Results and Discussion

The best fit between the observed and calculated intensities is shown in Figure 6, where the observed intensities were displayed as curves and calculated ones as discrete points since only a limited number of intensity data were used in the model fitting. The structure parameters corresponding to this fit are given in Table I. As can be seen in Figure 6, good agreement between the experimental and theoretical SAXS intensities has been

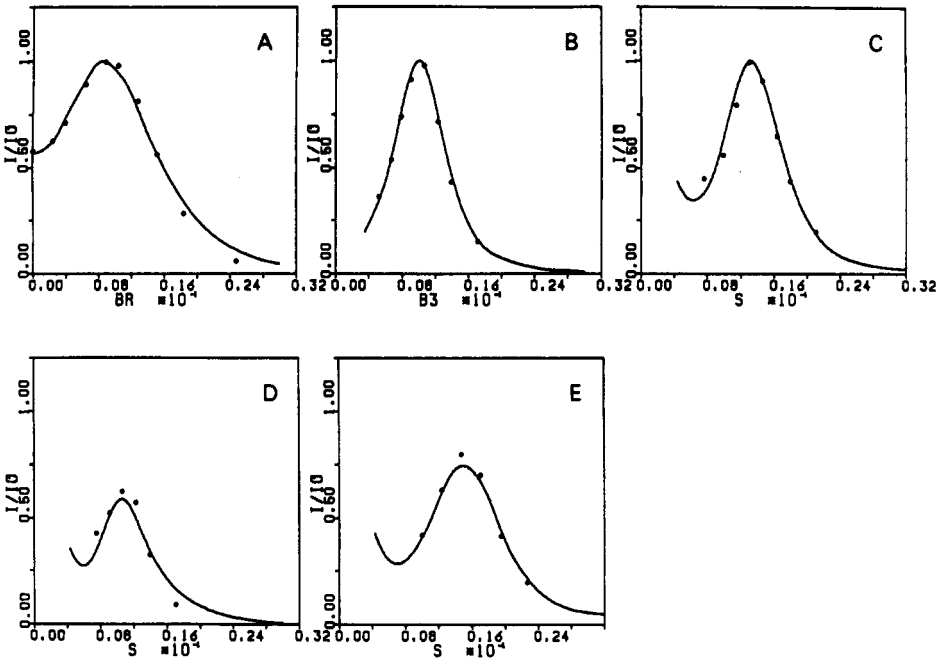

Figure 6. Best fit between the experimental and theoretical SAXS profiles of sections A–E for the nylon 6 fiber (normalized with the peak intensity, the abscissa in Å^{-1}).

Table I
Superstructure Parameters of the Nylon 6 Fiber Obtained by Least-Squares Fitting[a]

a_3, Å	80.7 ± 0.8	g_{rr}	0.20 ± 0.02
a_r, Å	89.4 ± 2.9	g_{33}	0.25 ± 0.005
β, deg	129.9 ± 0.7	g_{3r}	0 (fixed)
D, Å	85.8 ± 1.7	σ_α, deg	18.4 ± 1.1
H, Å	33.8 ± 1.0	σ_d, deg	73.8 ± 3.3
g_{r3}	0.48 ± 0.02	paracrystallinity	0.39

[a] a_3, long period; a_r, lateral distance between lamellae, equal to a_2 and $a_1 \sin\beta$; β, angle between $\mathbf{a}_1$ and $\mathbf{a}_3$ axes; D, lateral dimension of the lamella, identical with L_2 and $L_1 \sin\beta$; H, lamella thickness in fiber direction, identical with L_3; g_{r3}, g_{rr}, g_{33}, and g_{3r}, relative fluctuation parameters defined by eq 15; σ_α, width of the distribution density $D(\alpha)$; σ_d, width of the distribution density $Q(\delta)$.

obtained, and reasonable results for the superstructure parameters in Table I are found as well.

The values of the lattice fluctuations $g_{rr} = 0.20$ and $g_{33} = 0.25$ are within the range generally expected for the distance fluctuation between neighboring crystallites.[4-7,13] In particular, the g_{33} value is consistent with the observation that only one meridional intensity maximum is present in the SAXS pattern.[9] The relatively large value of $g_{r3} = 0.48$ is compared with 0.50 obtained for hot-stretched linear polyethylene[1] and 0.40 for cold-drawn isotactic polypropylene.[3] The values as high as g_{r3} obtained here have also been observed for other fluctuation parameters.[3-5,7] In the course of least-squares fitting, the minimum fluctuation parameter set,[6,25] in which the fluctuation components in $\mathbf{a}_r$ and $\mathbf{a}_2$ directions are assumed to be the same (see Figure 4) because of the rotational symmetry about the fiber axis and g_{3r} is set to zero, was utilized. With regard to g_{3r}, it was confirmed that the same value of $g_{3r} = 0$ could be obtained likewise, even if it was made independent and given a nonzero initial value. Since the fluctuation can be thought of as the relative displacement of crystallites (lamellae) within or between lamellar stacks, the resultant values for the fluctuation parameters, i.e., g_{3r} of zero value, large g_{r3}, and usual g_{33}, indicate that in the case of the nylon 6 fiber studied, the correlation between lamellae in different lamellar stacks is weak as compared with that between those within the same stack[5] and hence the sample may presumably assume the so-called "nematiclike" or fibrillar structure.[4]

The obtained value of $\sigma_\alpha = 18.4°$, which is half-height width of the Gaussian distribution $D(\alpha)$ of $\mathbf{n}$ with respect to $\mathbf{f}$ introduced by Wilke et al.,[12,13] is well compared with that assumed for highly oriented low-density polyethylene,[6] for which σ_α was expected to be in the range 10–20°. Since the distribution $Q(\delta)$ of $\mathbf{a}_1$ about $\mathbf{n}$, the half-height width σ_d of it equal to 73.8°, is newly introduced in this study, no information about it has ever been obtained. It is found, however, that setting σ_d to infinity (reducing to Wilke's model) leads to a serious discrepancy between the experimental and theoretical intensities of section E as well as a larger value of β required to fit the experimental pattern, whereas at the other extreme $\sigma_d = 0$ causes section A to deviate largely from the experimental intensity, while leading to a smaller β to fit the experimental pattern. According to Keller's model, the value of β should be responsible for the splitting angle of the diffraction lobes in the SAXS pattern. The β value (129.9°) obtained in Table I proves to be so. From the above observation, the resulting σ_d value, which gives rise to appropriate fit and allowable results for relevant parameters, may be considered to be reasonable.

The macrocrystallinity,[6] calculated from the dimensions of the lamella (D and H) and macrolattice (a_r and a_3), is 0.39, which agrees well with the experimental value, 0.36, based on the observed density of the fiber. The agreement becomes better if allowance is made for the existence (probably a few percent) of voids in the sample, which is indicated by the diffuse scattering on the equator.[21] It has been confirmed that this scattering can be completely excluded from the SAXS pattern by swelling the fiber with a solvent (e.g., benzyl alcohol) having density close to that of the amorphous part of the fiber. It should be added, nevertheless, that the SAXS pattern due to the density fluctuation between the amorphous and crystalline phases is not affected by the diffuse scattering because it attenuated steeply in the meridional direction. Such a scattering has also been observed for other fibers.[26,27]

While Keller's model gives the most intuitive but qualitative explanation of the four-point SAXS diagram,

Hosemann's allows quantitative information to be drawn from the SAXS intensity. In the model proposed here the consideration of the paracrystalline macrolattice by Hosemann is adopted. On this basis, the consideration of Keller, i.e., lamellar structure with inclined surface, is incorporated. In the case of the nylon 6 fiber under investigation, the SAXS pattern was best approached by such a combination of Hosemann's model with Keller's, giving reasonable superstructure parameters.

Model calculations[28] show that when the inclined lamellae are replaced by the "rectangular" ones for a monoclinic lattice, as in Wilke's model,[6] the intensity on the meridian increases appreciably because the Fourier transform of the lamella is redistributed from being populated in a direction deviating from **n** to being populated on it. With relation to the effect of σ_d on the fiber average intensity, it is shown that apart from the detailed intensity profiles of the 001 reflection, conspicuous change is observed for higher order reflections, which become weak or even disappear as σ_d increases, since the order of the superstructure decreases with increasing σ_d. Model calculations also reveal that the lateral dimension of crystallites (D) influences in an opposite manner the sensitivity of the intensity distribution to the inclination of the lamella surface and to the cluster distribution density $Q(\delta)$; a smaller lateral dimension, hence a broader Fourier transform, makes the intensity distribution less sensitive to the inclination but more sensitive to the density $Q(\delta)$ and vice versa. Besides, it can easily be imagined that the effect of the distribution function $Q(\delta)$ increases as the distribution function $D(\alpha)$ becomes broader.

It is a general consideration[29] that the lateral surfaces are parallel to the axes of molecular chains. So, by introducing Keller's model, the physical meanings of the distribution density $D(\alpha)$ and angle β become more clear: $D(\alpha)$ may also be considered to be the distribution of orientation of the molecular chains in the crystalline phase, and β is the angle between the chain axis and the lamellar surface. In addition, by choosing the $\mathbf{a}_1$ axis of the macrolattice parallel to the lamella surface and the $\mathbf{a}_3$ axis parallel to the direction of the molecular chains, as depicted in Figure 1, the choice of a monoclinic lattice for interpretation of the four-point reflection effect would become more convincing.

As has been mentioned above, if the half-height width σ_d of the distribution function $Q(\delta)$ (eq 7) approaches infinity, our model will reduce to Wilke's[6,12,13] except for the structure of the crystallite, i.e., cylinder or lamella with inclination, though the final expressions for the experimentally accessible intensity $I(r^*, \theta^*)$ differ largely from each other. As compared with Wilke's,[12] our derivation procedure for $I(r^*, \theta^*)$ is intuitive and the form of the final expression is relatively suitable to numerical calculation. Moreover, our model is still capable of producing a four-point diagram[28] for $\beta \neq 90°$, even if the distribution density $D(\alpha)$ is not centered at $\alpha_0 = 0$ but at a relatively large α_0 where Wilke's model has no longer been capable.

Using the model presented here, the quantitative study on the superstructure of nylon 6 fibers that suffered heat treatment at different temperatures and swelling in solvent mixtures of different concentrations is in progress in our laboratory and will be reported elsewhere.

Appendix

Scattered Amplitude by Lamellae with Inclined Surfaces. The coordinate system (x, y, z) in real space is defined such that the center of the lamella is located at the origin, the y axis is parallel to L_2, and the z axis is parallel to L_3, as shown in Figure 7. The reciprocal system

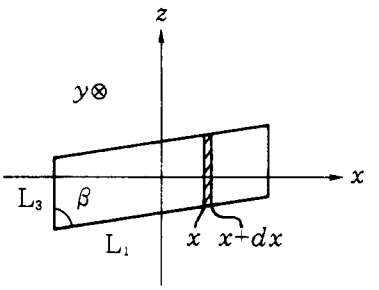

Figure 7. Lamella with inclined surfaces. The y axis is perpendicular to the paper plane.

(X, Y, Z) is defined in the same orientation. The lamella can then be described by the following parallelpiped:

$$-\frac{L_1}{2}\sin\beta \le x \le \frac{L_1}{2}\sin\beta \tag{A-1a}$$

$$-\frac{L_2}{2} \le y \le \frac{L_2}{2} \tag{A-1b}$$

$$-\frac{L_3}{2} + x\cot\beta \le z \le \frac{L_3}{2} + x\cot\beta \tag{A-1c}$$

Assuming a constant density of unity within the lamella and zero outside, therefore, the Fourier transform $F(S)$ of such an entity can be written as

$$F(S) \equiv F(XYZ) = \int_{-(L_3/2)+x\cot\beta}^{(L_3/2)+x\cot\beta}\int_{-L_2/2}^{L_2/2}\int_{-(L_1/2)\sin\beta}^{(L_1/2)\sin\beta} e^{2\pi i(xX+yY+zZ)}\,dx\,dy\,dz \tag{A-2}$$

Before calculating the integral, several fundamental equations have to be worked out. First, the following equation holds:[24]

$$\int_{-H/2}^{H/2} e^{2\pi ixX}\,dx = \frac{\sin\pi HX}{\pi X} \tag{A-3}$$

In the light of eq A-3, we have, setting $y = x - H/2$

$$\int_0^H e^{2\pi ixX}\,dx = \int_{-H/2}^{H/2} e^{2\pi i(y+(H/2))X}\,dy = e^{\pi iHX}\int_{-H/2}^{H/2} e^{2\pi iyX}\,dy = e^{\pi iHX}\frac{\sin\pi HX}{\pi X} \tag{A-4}$$

and, setting $y = x - H_1$ followed by $H = H_2 - H_1$

$$\int_{H_1}^{H_2} e^{2\pi ixX}\,dx = \int_0^{H_2-H_1} e^{2\pi i(y+H_1)X}\,dy = e^{2\pi iH_1X}\int_0^{H_2-H_1} e^{2\pi iyX}\,dy = e^{2\pi iH_1X}e^{\pi iHX}\frac{\sin\pi HX}{\pi X} \tag{A-5}$$

In order to conduct the foregoing integration (eq A-2), we rewrite it as

$$F(XYZ) = \int_{-L_2/2}^{L_2/2} e^{2\pi iyY}\,dy \times \int_{-(L_1/2)\sin\beta}^{(L_1/2)\sin\beta} e^{2\pi ixX}\int_{-(L_3/2)+x\cot\beta}^{(L_3/2)+x\cot\beta} e^{2\pi izZ}\,dz\,dx = A\int_{-(L_1/2)\sin\beta}^{(L_1/2)\sin\beta} Be^{2\pi ixX}\,dx \tag{A-6}$$

where

$$A = \int_{-L_2/2}^{L_2/2} e^{2\pi iyY}\,dy \tag{A-7}$$

and

$$B = \int_{-(L_3/2)+x\cot\beta}^{(L_3/2)+x\cot\beta} e^{2\pi izZ}\,dz \tag{A-8}$$

In terms of eq A-3 and A-5, eq A-7 and A-8 become

$$A = \frac{\sin \pi L_2 Y}{\pi Y} \tag{A-9}$$

and

$$B = e^{2\pi i(-(L_3/2)+x\cot\beta)Z} e^{\pi i L_3 Z} \frac{\sin \pi L_3 Z}{\pi Z} = e^{2\pi i x Z \cot\beta} \frac{\sin \pi L_3 Z}{\pi Z} \tag{A-10}$$

respectively. Finally, inserting (A-9) and (A-10) into (A-6) gives

$$F(XYZ) = \frac{\sin \pi L_2 Y}{\pi Y} \frac{\sin \pi L_3 Z}{\pi Z} \int_{-(L_1/2)\sin\beta}^{(L_1/2)\sin\beta} e^{2\pi i x(X+Z\cot\beta)}\, dx$$
$$= \frac{\sin [\pi L_1 \sin \beta(X + Z \cot \beta)]}{\pi(X + Z \cot \beta)} \frac{\sin \pi L_2 Y}{\pi Y} \frac{\sin \pi L_3 Z}{\pi Z} =$$
$$\frac{\sin [\pi L_1(X \sin \beta + Z \cos \beta)]}{\pi(X \sin \beta + Z \cos \beta)} \frac{\sin \pi L_2 Y}{\pi Y} \frac{\sin \pi L_3 Z}{\pi Z} \sin \beta \tag{A-11}$$

Further, by taking the approximation in terms of the Gaussian function[13]

$$\frac{\sin^2 (\pi X)}{(\pi X)^2} \doteq \exp(-\pi X^2) \tag{A-12}$$

the final expression for the amplitude $F(S)$, eq A-11, can be rewritten as (relative unit)

$$|F(S)|^2 = \exp\{-\pi[L_1^2(X \sin \beta + Z \cos \beta)^2 + L_2^2 Y^2 + L_3^2 Z^2]\} \sin^2 \beta \tag{A-13}$$

where $S = (X^2 + Y^2 + Z^2)^{1/2}$ is the scattering vector in reciprocal space.

References and Notes

(1) Čačkovič, J. L.; Hosemann, R.; Čačkovič, H. *Kolloid Z. Z. Polym.* **1971**, *247*, 824.
(2) Hosemann, R.; Čačkovič, J. L.; Sassoui, M.; Weick, D. *Prog. Colloid Polym. Sci.* **1979**, *66*, 143.
(3) Čačkovič, J. L.; Hosemann, R.; Čačkovič, H.; Ferrero, A.; Ferracini, E. *Polymer* **1976**, *17*, 303.
(4) Ferrero, A.; Ferracini, E.; Čačkovič, J. L.; Čačkovič, H. *J. Polym. Sci., Polym. Phys. Ed.* **1984**, *22*, 485.
(5) Fronk, W.; Wilke, W. *Colloid Polym. Sci.* **1983**, *261*, 1010.
(6) Fronk, W.; Wilke, W. *J. Polym. Sci., Polym. Phys. Ed.* **1986**, *24*, 839.
(7) Ferracini, E.; Ferrero, A.; Čačkovič, J. L.; Hosemann, R.; Čačkovič, H. *J. Macromol. Sci.-Phys.* **1974**, *B10*, 97.
(8) Bonart, R.; Hosemann, R. *Kolloid Z. Z. Polym.* **1962**, *186*, 16.
(9) Hosemann, R.; Bagchi, S. N. *Direct Analysis of Diffraction by Matter*; North-Holland: Amsterdam, 1962.
(10) Kaji, K.; Mochizuki, T.; Akiyama, A.; Hosemann, R. *J. Mat. Sci.* **1978**, *13*, 972.
(11) Hosemann, R.; Čačkovič, J. L.; Kaji, K. *J. Appl. Crystallogr.* **1978**, *11*, 540.
(12) Wilke, W.; Göttlicher, K. *Colloid Polym. Sci.* **1981**, *259*, 596.
(13) Fronk, W.; Wilke, W. *Colloid Polym. Sci.* **1985**, *263*, 97.
(14) Hay, I. L.; Keller, A. *J. Mat. Sci.* **1967**, *2*, 538.
(15) Grubb, D. T.; Dlugosz, J.; Keller, A. *J. Mat. Sci.* **1975**, *10*, 1826.
(16) Keller, A.; Pope, D. P. *J. Mat. Sci.* **1971**, *6*, 453.
(17) Pope, D. P.; Keller, A. *J. Polym. Sci., Polym. Phys. Ed.* **1975**, *13*, 533.
(18) Gerasimov, V. I.; Tsvankin, D. Y. *Polym. Sci. USSR* **1969**, *11*, 3013.
(19) Gezalov, M. A.; Kuksenko, V. S.; Slutsker, A. I. *Polym. Sci. USSR.* **1970**, *12*, 2027.
(20) Crist, B. *J. Appl. Crystallogr.* **1979**, *12*, 27.
(21) Zheng, Z.; Nojima, S.; Yamane, T.; Ashida, T. *Polym. J.* **1989**, *21*, 65.
(22) Hall, I. H. *Structure of Crystalline Polymers*; Elsevier: England, 1984.
(23) Matyi, R. J.; Crist, B. *J. Polym. Sci., Polym. Phys. Ed.* **1978**, *16*, 1329.
(24) Vainshtein, B. K. *Diffraction of X-Rays by Chain Molecules*; Elsevier: Amsterdam, 1966.
(25) Wilke, W. *Acta Crystallogr.* **1983**, *A39*, 864.
(26) Dobb, M. G.; Johnson, D. J.; Majeed, A.; Saville, B. P. *Polymer* **1979**, *20*, 1284.
(27) Hindeleh, A. M.; Halim, N. A.; Ziq, K. A. *J. Macromol. Sci.-Phys.* **1984**, *B23*, 289.
(28) Zheng, Z. Thesis, 1989.
(29) Flory, P. J. *J. Am. Chem. Soc.* **1962**, *84*, 2857.

One-Dimensional Aromatic Crystals in Solution. 10. A Helical Array of Anthryl Groups along a Polypeptide Chain

Masahiko Sisido†

Research Laboratory of Resources Utilization, Tokyo Institute of Technology, 4259 Nagatsuta, Midori-ku, Yokohama 227, Japan.

Received February 9, 1989; Revised Manuscript Received March 30, 1989

ABSTRACT: A sequential polypeptide having a repeating unit of [Lys(Z)-Lys(Z)-9-antAla] was synthesized [Lys(Z) = $^{\epsilon}N$-(benzyloxycarbonyl)-L-lysine; 9-antAla = L-9-anthrylalanine]. Circular dichroism of the polypeptide in solution showed a typical pattern of right-handed α-helix at the amide absorption region. A very strong exciton splitting ($\Delta\epsilon_{248} = -217$; $\Delta\epsilon_{261} = +525$) was observed at the ^{1}Bb absorption band of the anthryl group. The conformational energy calculation and the theoretical CD calculation indicated a one-dimensional array of the anthryl chromophores along the α-helical main chain. The interchromophore center-to-center distance was predicted to be 7.2 Å. No strong ground-state interaction, such as dimer formation, was detected in the absorption and the fluorescence excitation spectra. Fluorescence spectra showed monomer and excimer fluorescence. It is suggested that very fast energy migration leads to efficient excimer formation.

Helical polypeptide chains have been used as the molecular framework along which a variety of chromophores can be arranged in a specific order and with specific spatial configurations.[1,2] Sequential polypeptides of the form I, containing L-1-naphthylalanine (napAla) [p(L_2N)][3] or L-1-pyrenylalanine (pyrAla) [p(L_2P)],[4] have been synthesized. The polypeptides were found to take α-helical main-chain conformations[5] and the side-chain chromophores were shown to be arranged regularly along the helix.

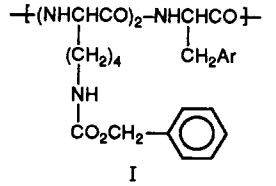

I

† Part of this work has been carried out at the Research Center for Medical Polymers and Biomaterials, Kyoto University.

0024-9297/89/2222-4367$01.50/0